Proceedings of 20th International Symposium on Music Acoustics
(Associated Meeting of the International Congress on Acoustics)

25-31 August 2010, Sydney and Katoomba, Australia

Glottal jet behaviour in a self-oscillating *in vitro* model of the vocal folds with downstream constrictions

Adam G. Apostoli, D. Murray Campbell, and Clive A. Greated

School of Physics and Astronomy, University of Edinburgh, Edinburgh, United Kingdom

PACS: 43.75.Rs, 43.70.Bk, 43.70.Jt

ABSTRACT

With the ventricular bands shown as having a direct impact on vocal fold oscillation (either inducing or hindering self-oscillation depending on their position), understanding the nature of their effect on the glottal jet may provide a useful insight into some voice pathologies. This paper describes a study using a three-times life size *in vitro* model of the vocal folds constructed from latex and water, which replicates basic features of the fluid-structure interactions that take place in the human larynx. Using Particle Image Velocimetry, it has been possible to study the nature of the glottal jet during steady state oscillation of the vocal folds with downstream constrictions. A key advance on previous studies in this area is the ability to now observe the glottal jet from the point at which it emerges from the vocal folds and for the case where no downstream constrictions are used. Finally, a comparison between the flow-field measurements and established theories on the expansion of the glottal jet is made.

INTRODUCTION

Within the larynx, complex soft tissue structures are made to oscillate periodically by an airflow generated by an overpressure in the lungs. Above the laryngeal ventricle are found two further structures, termed the ventricular bands or false vocal folds. These structures are like the vocal folds but have been observed to have a lower stiffness and be more viscous (Agarwal 2004). In contrast to the vocal folds, due to having these unique properties the ventricular bands have been identified as being poor vibrators. In previous studies, the ventricular bands have been observed playing an important role in certain types of musical styles, in particular Mongolian and Tibetan throat-singing and, from the Western tradition, Sardinian Cantu *A Tenore* (Henrich et al. 2006). Although a limited amount of work has been undertaken on the ventricular bands (Agarwal et al. 2003), with more being undertaken more recently, their effect in phonation is surprisingly still not fully understood (Bailly et al. 2008).

From recent studies, it is known that the interaction between the vocal folds and the ventricular bands is caused by the aerodynamic interaction of the glottal jet with the ventricular bands, with a pressure recovery at the ventricular bands due to flow reattachment (Bailly et al. 2008, Bailly 2009, Newton 2009). Due to the difficulty of accessing the larynx for scientific study, these earlier studies have been based on simplified models of the human larynx, so that pressure taps or indeed powerful lasers, like the kind used for Particle Image Velocimetry (PIV), can be introduced, both of which would not be possible in an *in vivo* environment. Another reason for using simplified models of the larynx is that control parameters of the model can be fixed, meaning that any observed phenomena can be fully attributed to particular control parameter settings and replicated without ambiguity. An obvious disadvantage of this approach is that measurements taken using the *in vitro* model rarely align precisely with measurements taken *in vivo*, meaning that it may not be possible to faithfully replicate all the detail observed in the voice. At best, these simplified models can be seen as a good first approximation, exhibiting the main functions and phenomena observed *in vivo*.

As has been identified by Agarwal, one of the best ways to understand the effect of the ventricular bands is to include them in current models that we have of the larynx (Agarwal et al. 2003). Following on directly from the work of Bailly and Newton (Bailly et al. 2008, Bailly 2009, Newton 2009), three theoretical hypotheses for the geometry of the glottal jet between the vocal folds and the ventricular bands are proposed and compared against preliminary flow-field measurements taken with and without downstream constrictions. The requirement to know the geometry of the glottal jet is very important for computational models, where a simplified description of the flow mechanics is used to calculate the aerodynamic forces which are applied to the ventricular bands.

JET EXPANSION THEORIES

In an attempt to better understand the way in which the glottal jet interacts with the ventricular bands and why certain effects, such as period-doubling oscillation of the ventricular bands, are observed three hypotheses for the expansion of the glottal jet are put forward. These jet expansion theories first appear in the work of Bailly (Bailly et al. 2008) and are covered in greater detail in (Bailly 2009, Newton 2009). For convenience, a summary of these jet expansion hypotheses is presented here. An assumption which is made in proposing these hypotheses is that the flow is two-dimensional. This assumption is made because the separation of the vocal folds in our *in vitro* model, expressed as the glottal width, is significantly smaller than the height of the glottis, which is typically an order of magnitude larger.

Uniform jet hypothesis

The first and simplest of these jet expansion theories is the uniform jet hypothesis. This hypothesis, illustrated in Figure 1, assumes that the width of the glottal jet at the point where it reattaches to the ventricular bands is the same as that at the point where the glottal flow separates from the walls of the vocal folds. Assuming that no expansion of the glottal jet occurs, this relation is expressed simply as

$$h_R = h_{s1}, \tag{1}$$

where h_R is the width of the glottal jet at the point of flow reattachment and h_{s1} is the width of the jet at the point of flow separation.

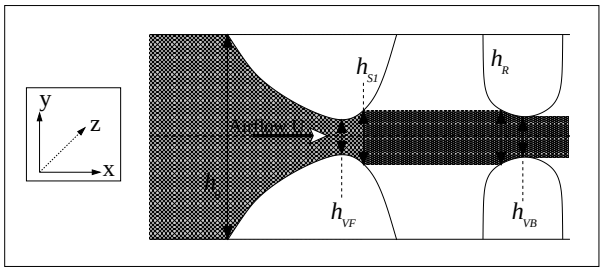

Source: Adapted from (Newton 2009)

Figure 1: Diagram illustrating the uniform jet expansion hypothesis, where h_0 is the width of the trachea, h_{VF} is the minimum glottal opening, h_{s1} is the point of flow separation, h_R is the point of flow reattachment, and h_{VB} is the minimum ventricular band separation.

Laminar jet hypothesis

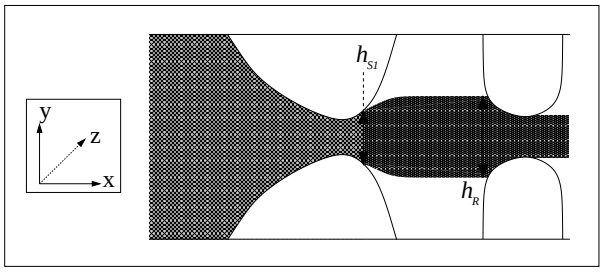

Source: Adapted from (Newton 2009)

Figure 2: Diagram illustrating the laminar jet expansion hypothesis, where h_{s1} is the point of flow separation and h_R is the point of flow reattachment.

The second proposed jet expansion theory is the laminar jet hypothesis. As observed in Figure 2, the glottal jet is shown to expand in a non-linear fashion as it approaches the point of reattachment at the ventricular bands. Modelling the glottal jet as a free shear layer and neglecting edge effects observed in confined jets, the glottal jet is seen to expand after flow separation up until a point where the jet then assumes a uniform profile. It is at this point that the pressure gradient across the jet in the x-direction reduces to zero, halting the jet expansion. Assuming that the jet grows under the influence of viscous diffusion and that the flow is self-similar, the equation governing this hypothesis is:

$$h_R = h_{s1} + 21.8\left(\frac{h_{s1}W_{VF}\mu^2\left(x_R - x_{s1}\right)^2}{U^2\rho^2}\right)^{\frac{1}{3}}, \tag{2}$$

where W_{VF} is the height of the glottis, μ is the dynamic viscosity, x_{s1} is the position of the point of flow separation along the x-axis, x_R is the position of the point of flow reattachment at the ventricular bands along the x-axis, U is the volume flow, and ρ is the density of the fluid.

Turbulent jet hypothesis

The final jet expansion hypothesis, seen in Figure 3, is the turbulent jet hypothesis. This hypothesis is based on the idea that

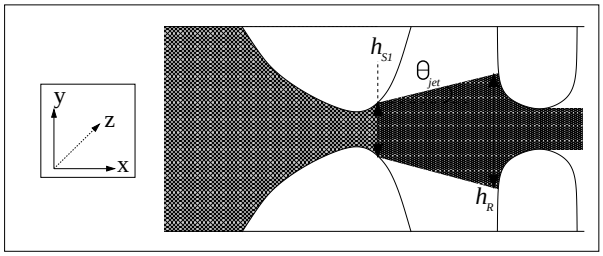

Source: Adapted from (Newton 2009)

Figure 3: Diagram illustrating the turbulent jet expansion hypothesis, where h_{s1} is the point of flow separation, h_R is the point of flow reattachment, and θ_{jet} is the half-angle of the jet expansion.

the Navier-Stokes equations, which govern instantaneous fluid flow, can be reduced down to the simplified Reynolds equations, which then allow us to model the glottal jet as a two-dimensional free turbulent jet. From this, it is shown that the jet grows linearly as x increases, which Kundu proved empirically had a half-angle slope $\left(\theta_{jet}\right)$ of 4° (Kundu et al. 2002). This relation is expressed in the equation

$$h_R = h_{s1} + 2.\tan 4^\circ.\left(x_2 - x_{s1}\right). \tag{3}$$

EXPERIMENTAL SETUP

A self-oscillating *in vitro* model of the vocal folds, which is about three-times life size, including a trachea and vocal tract with and without downstream constrictions was used for this study. Each of the vocal folds was created from an aluminium block, with an edge cut at the top forming a 38° angle with the topside of the block. Out of this edge a half-circle was cut with a diameter of 20mm over which sheet latex of 0.2mm thickness is stretched and glued into place. Through holes drilled into the blocks, the cavities in the vocal fold blocks were then connected to a head of water, via flexible tubing, which then filled the cavities and allowed the vocal folds to assume their initial or resting shape.

The vocal fold blocks were then mounted into an outer casing, produced from perspex, glass, and polycarbonate, which was then sealed, so as to be air-tight. The polycarbonate front plate used on the vocal fold model casing was specially designed to support a free-standing vocal tract and to allow as much optical access as possible. Careful adjustment of the height of the head of water was used to determine the pressure of water within the vocal folds. This was an important control parameter in the experiment, as it allowed for the control of the stiffness of the vocal folds and hence to make adjustments to the frequency at which the vocal folds were oscillating.

The vocal fold model was connected to a 15.3cm long perspex trachea, which was attached to a large wooden box, modelling the lungs. This box had a volume of approximately 1m^3 and was lined with acoustically absorbing foam, so as to minimise any possible upstream acoustic resonance and to maintain a constant upstream pressure. Connected to the downstream part of the vocal fold model was one of two glass vocal tracts, one with downstream constrictions and the other without. The glass vocal tracts were hollow cuboidal structures which were 58mm long and 20mm wide (internally). This specific geometry was chosen so that optical distortion caused through the use of curved surfaces would be avoided. The downstream constrictions, a simplified representation of the ventricular bands, were built from aluminium and had a semi-circular top with a radius of 5mm and flat sides extending down to the walls of the vo-

cal tract. The separation between the minimum opening of the two constrictions (h_{VB}) was 3mm and the constrictions were placed 16mm downstream of the entrance to the vocal tract.

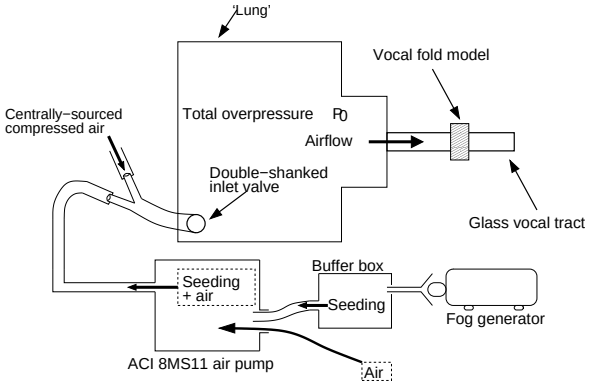

Source: Adapted from (Newton 2009)

Figure 4: Schematic diagram of the pressure and seeding delivery systems and the *in vitro* model used in this study.

Connected to the 'lung' through a double-shanked valve was the seeding and air pressure supplies. A schematic diagram of these two systems in the experimental setup can be seen in Figure 4. The seeding for the PIV experiments was provided from a Safex fog generator, where the seeding was created from a mix of alcohol and water with a mean particle size measuring 1μm in diameter. These particles were delivered to the 'lung' from a buffer box and via an air pump to control the density of fog particles throughout the experiment. Connected to the second inlet of the double-shanked valve was a compressed air pressure source, which was supplied centrally from a compressor and controlled within the laboratory. To measure the static pressure upstream of the vocal folds (P_0) a digital manometer was connected through a hole made in the upper wall of the trachea and placed 1cm downstream of the entrance.

A copper vapour laser was used as the illumination source, delivering approximately 6-10 mJ per pulse. The laser beam was delivered via a fibreoptic cable and then expanded into a thin sheet, approximately 1-2mm thick, using an Oxford Lasers Fibresheet. Due to the power of the laser, the entire model and light sheet arrangement, once set up, was enclosed in a metal housing to protect the user. A PCO Double Shutter camera, with a resolution of 1280 $\times$ 1024 pixels, was used to capture the PIV image pairs. The PIV images were all analysed in Dantec's DynamicStudio software, then exported to MATLAB for later analysis.

For synchronising the PIV measurements to the acoustic signal of the self-oscillating model, the acoustic pressure upstream of the vocal folds was sampled using a Bruël and Kjær 4192 condenser microphone attached to a short probe fitting. This probe microphone setup was placed on the upper wall of the trachea 1cm upstream of the vocal folds. The upstream acoustic pressure signal was then passed to a custom-built zero-crossing detector which was used in conjunction with a delay generator to coordinate the acquisition of the PIV image pairs at different phase steps in the acoustic cycle. When the vocal tract with downstream constrictions was introduced, the second harmonic in the upstream acoustic pressure became so strong that a second zero-crossing within the acoustic cycle was detected. To combat this, an active band-pass filter was used. This filter was calibrated for every run on an oscilloscope so that the zero-crossings of the fundamental frequency of filtered and unfiltered signals coincided.

To record the filtered and unfiltered microphone signals and the pulses from the zero-crossing detector and to send timings to the delay generator, data acquisition hardware and software built in LabVIEW were used. These recorded signals were all later used to synchronise the image pair acquisitions with the acoustic cycle, making it possible to assess how the image pairs were distributed when aligned to the acoustic cycle. To help reduce the impact of problems typically encountered in PIV with glare, any non-necessary surface was painted black and the image mean removed from each run.

RESULTS

In the results which follow, 10 runs of 40 image pair acquisitions were taken for the setup with a vocal tract containing downstream constrictions and also without. Taking the period of the fundamental frequency of the upstream acoustic pressure signal taken as the model's acoustic cycle, the cycle was split up into 10 phase steps. Each run of 40 image pair acquisitions was taken at 1 of these phase steps, allowing a mean flow-field to be calculated for each step, greatly simplifying the analysis process. In addition, as the position of each phase step within the acoustic cycle is known, these can later be linked to the model's geometry and open area if the relationship between the acoustic and phonatory cycles is found. Tables 1 and 2 show the mean time of the image pair acquisitions in each phase step along with the standard deviation of these image pair acquisitions.

Phase Step	Mean (s)	Standard Deviation (s)
1	5.21×10^{-5}	8.41×10^{-6}
2	5.49×10^{-4}	1.12×10^{-5}
3	1.05×10^{-3}	1.13×10^{-5}
4	1.56×10^{-3}	1.25×10^{-5}
5	2.07×10^{-3}	9.05×10^{-6}
6	2.58×10^{-3}	1.20×10^{-5}
7	3.09×10^{-3}	1.05×10^{-5}
8	3.59×10^{-3}	9.91×10^{-6}
9	4.10×10^{-3}	1.17×10^{-5}
10	4.61×10^{-3}	1.03×10^{-5}

Table 1: Table showing the the mean and standard deviation of image pair acquisition times for each phase step in PIV runs on a model without downstream constrictions. The rounded fundamental frequency (f_0) for this setup was 196Hz.

Phase Step	Mean (s)	Standard Deviation (s)
1	5.24×10^{-3}	5.40×10^{-5}
2	4.97×10^{-4}	3.96×10^{-5}
3	1.06×10^{-3}	5.75×10^{-5}
4	1.61×10^{-3}	5.37×10^{-5}
5	2.17×10^{-3}	5.10×10^{-5}
6	2.72×10^{-3}	5.28×10^{-5}
7	3.26×10^{-3}	5.52×10^{-5}
8	3.83×10^{-3}	5.71×10^{-5}
9	4.37×10^{-3}	4.74×10^{-5}
10	4.94×10^{-3}	4.93×10^{-5}

Table 2: Table showing the the mean and standard deviation of image pair acquisition times for each phase step in PIV runs on a model with downstream constrictions. The rounded fundamental frequency (f_0) for this setup was 180Hz.

These tables show that the phase steps are equally distributed with small standard deviations. A noticeable difference between the two tables is that the standard deviation of image pair acquisitions for the setup with downstream constrictions in the vocal tract are, on average, 3 or 4 times larger than those for the setup without downstream constrictions. The most logical

explanation for this is that the vocal fold oscillation for this particular configuration was less stable, assuming a wider range of fundamental frequencies, which the image pair acquisition synchronisation system does not correct for. In the case of the setup with downstream constrictions, this instability may have been compounded through the use of the band-pass filter. Also, in Table 2, the mean for phase step 1 is much larger than that in the equivalent phase step in Table 1. This is most probably due to the rounded fundamental frequency (f_0), used for synchronisation, being slightly higher than the actual fundamental frequency of the model. As can be seen in the standard deviation of image pair acquisitions, this has not affected the distribution of image pair acquisitions but only the position of the mean.

Throughout the PIV runs, the upstream pressure (P_0) remained constant at 1.24kPa and the head of water kept at 28cm, exerting a pressure of 2.8kPa on the vocal folds. The jet widths were extracted from the calculated mean of the flow-field measurements for each phase step. This was taken to be the distance between the closest point each side of the peak vertical velocity component where the magnitude is half of that at the peak. For comparison, jet widths for three analysis lines across all phase steps are presented for both configurations, along with jet widths across the vast majority of the observed jet. Unfortunately, due to fogging around the downstream constrictions as the runs progressed, the jet widths are only considered from 0.4mm to 12.5mm downstream of the vocal folds.

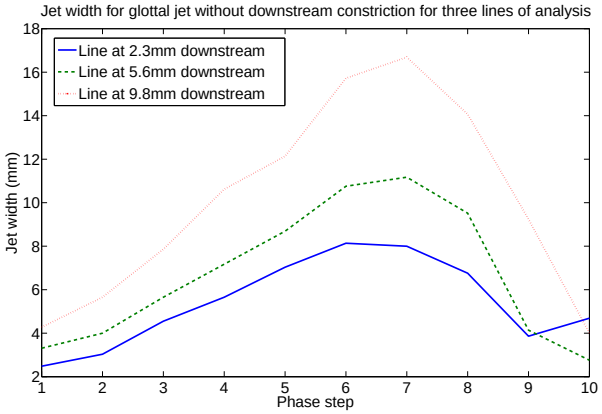

Figure 5: Jet width extracted from flow-field measurements across three lines of analysis for a setup without downstream constrictions.

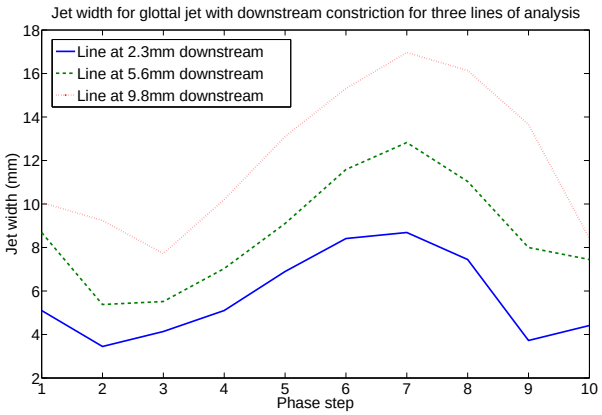

Figure 6: Jet width extracted from flow-field measurements across three lines of analysis for a setup with downstream constrictions.

Shown in Figures 5 and 6 is the evolution of the jet width for setups with and without downstream constrictions across three lines of analysis. The three lines, indicated in the legend, are: 2.3mm, 5.6mm, and 9.8mm downstream of the vocal folds. What can be seen from these two graphs is that, on average, the jet width appears to change linearly with the open area of the vocal folds. In addition, the jet widths for both the setup with and without downstream constrictions behave in similar ways, with peak jet widths in the same phase step and of a similar value. A noticeable difference between the two configurations is the jet widths over phase steps 1 and 2, which are higher in the case with downstream constrictions than without.

When considering the jet expansion hypotheses discussed earlier, it is immediately apparent that the uniform hypothesis is not supported by either of these two graphs, as the value of the jet width from one analysis line to next increases in value rather than remaining the same. In contrast though, the turbulent jet hypothesis looks more promising. Taking jet widths at phase steps 4 and 7 and, considering that the expansion is linear, putting the jet width for the analysis line at 5.6mm into the jet hypothesis equation in an attempt to predict the jet width at 9.8mm, produces values which are too high. It is not possible to see for these graphs whether or not the laminar jet expansion hypothesis is supported.

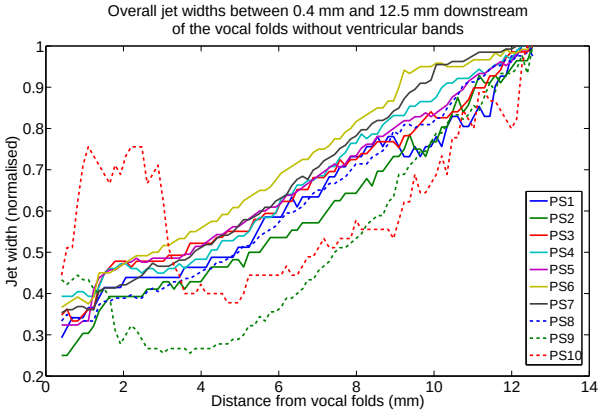

Figure 7: Normalised jet widths extracted from flow-field measurements from 0.4mm to 12.5mm downstream of the vocal folds for a configuration without downstream constrictions.

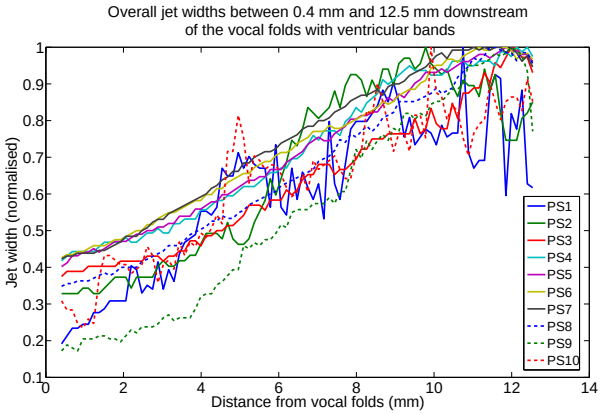

Figure 8: Normalised jet widths extracted from flow-field measurements from 0.4mm to 12.5mm downstream of the vocal folds for a configuration without downstream constrictions.

Figures 7 and 8 are plots of the jet widths for all ten phase steps for all data between 0.4mm and 12.5mm downstream of the vocal folds for both configurations with and without downstream constrictions. The jet width values have been normalised, so as to allow any general trends between different phase steps to be identified more easily. The first point to note is that the ma-

jority of the normalised jet widths for both configurations approximately follow a straight line of a similar gradient. Some obvious exceptions to this are phase steps 9 and 10 from Figure 7 and phase steps 1, 9, and 10 from Figure 8.

A further problem can be seen in Figure 7, where a sharp rising slope appears briefly in the majority of phase steps at around 1.6mm downstream of the vocal folds. A possible explanation for this could be the proximity of the flow at this point to the vocal folds and possible glare caused by laser light becoming refracted from the surface of the vocal fold latex. Concerning ourselves once again with the jet expansion theories discussed earlier, it is very obvious that neither the uniform or the laminar jet expansion hypotheses are supported by our results. The turbulent jet hypothesis is supported by the jet widths shown in Figures 7 and 8; however, it has been shown that predictions made using the turbulent jet hypothesis were too large when compared with measured data.

CONCLUSION AND FUTURE WORK

In the course of this paper, three theoretical hypotheses to explain the expansion of the glottal jet, as it emerges from the vocal folds with downstream constrictions, have been proposed and summarised. Using Particle Image Velocimetry, the jet from a self-oscillating *in vitro* model of the vocal folds with and without downstream constrictions in the vocal tract has been studied. A key advance of this study has been the ability to obtain flow-field measurements of the glottal jet as it emerges from the vocal folds, allowing the jet width to be extracted much further upstream than before.

The jet widths for three lines of analysis have been plotted for configurations with and without downstream constrictions, along with normalised jet widths from all flow-field data between 0.4mm and 12.5mm downstream of the vocal folds. Conclusions from analysis of these results found that the uniform and laminar jet expansion hypotheses were not supported by trends observed, but that the turbulent jet expansion hypothesis was the most plausible. This was supported by the observation that the overall jet expansion seen was approximately linear. However, a problem identified with this theory was that when making predictions for the jet width from one analysis line to the next, the value acquired was consistently too large.

The results presented in this paper are preliminary and are only the first step towards investigating the true nature of the glottal jet and its behaviour in the presence of downstream constrictions. Further work will consist of more flow-field measurements being taken for these two configurations. Also, it is anticipated that flow-field measurements will be taken for downstream constrictions placed at different positions and with different degrees of separation, the jet expansion hypotheses then being compared to the experimentally acquired jet widths. Finally, it is our intention to compare jet widths gathered from flow-field measurements to simulations made on a lumped element two-mass model of the vocal folds with downstream constrictions.

ACKNOWLEDGEMENTS

The authors would like to thank Dantec Dynamics A/S for the use of their DynamicStudio software, which was used to process the PIV data presented in this paper. The authors also gratefully acknowledge the financial support of COST Action 2103 through a Short Term Scientific Mission and the Engineering and Physical Sciences Research Council (EPSRC).

REFERENCES

M. Agarwal. *The false vocal folds and their effect on translaryngeal airflow resistance*. PhD thesis, Bowling Green State University, OH, 2004.

M. Agarwal, R. C. Scherer, and H. Hollien. The False Vocal Folds: Shape and Size in Frontal View During Phonation Based on Laminagraphic Tracings. *Journal of Voice*, 17(2): 97–113, 2003.

L. Bailly. *Interaction entre cordes vocales et bandes ventriculaires en phonation: exploration in-vivo, modélisation physique, validation in-vitro*. PhD thesis, École Doctorale de L'Université du Maine, 2009.

L. Bailly, X. Pelorson, N. Henrich, and N. Ruty. Influence of a constriction in the near field of the vocal folds: Physical modeling and experimental validation. *The Journal of the Acoustical Society of America*, 124(5):3296–3308, 2008.

N. Henrich, B. Lortat-Jacob, M. Castellengo, L. Bailly, and X. Pelorson. Period-doubling occurences in singing: the 'bassu' case in traditional Sardinian 'A Tenore' singing. In *International Conference on Voice Physiology and Biomechanics, Tokyo, Jul*, 2006.

P. K. Kundu, I. M. Cohen, and H. H. Hu. *Fluid Mechanics*. Academic Press, 2nd edition, 2002.

M. J. Newton. *Experimental Mechanical and Fluid Mechanical Investigations of the Brass Instrument Lip-reed and the Human Vocal Folds*. PhD thesis, School of Physics and Astronomy; University of Edinburgh, 2009.